Supporting Information

Electrochemical Reduction of Nitrate to Hydroxylamine on Gold Electrode

Yangshan Xie,[a] Michiel De Ras,[b] Jiwu Zhao,[c,d] Tianxi Liu,[e] Feili Lai,[e] Johan Hofkens,[b,f] Maarten B.J. Roeffaers,[*a]

[a]Centre for Membrane Separations, Adsorption, Catalysis, and Spectroscopy for Sustainable Solutions, Department of Microbial and Molecular Systems, KU Leuven Celestijnenlaan 200F, 3001 Leuven, Belgium.

[b]Molecular Imaging and Photonics, Department of Chemistry, KU Leuven, Celestijnenlaan 200F, Leuven, 3001, Belgium

[c]State Key Laboratory of Photocatalysis on Energy and Environment, College of Chemistry, Fuzhou University, Fuzhou, 350116 China

[d]Division of Physical Sciences and Engineering, King Abdullah University of Science and Technology (KAUST), Thuwal, 23955–6900 Saudi Arabia

[e]*The Key Laboratory of Synthetic and Biological Colloids, Ministry of Education, School of Chemical and Material Engineering, International Joint Research Laboratory for Nano Energy Composites, Jiangnan University, Wuxi, China*

[f]Max Plank Institute for Polymer Research, Mainz, D-55128, Germany.

[*]Corresponding author: E-mail address: maarten.roeffaers@kuleuven.be

Experimental Details

1. Chemicals

Chemicals: Gold wire (99.999%, 0.5mm diameter), absolute ethanol (C_2H_5OH), nitric acid (HNO_3), sulfuric acid (H_2SO_4), hydroxylammonium chloride ($NH_2OH•HCl$) and ammonia standard solution (1000 ppm), potassium nitrate (KNO_3), potassium nitrite (KNO_2), hydroxylamine solution (NH_2OH, 50 wt. % in H_2O), deionized water (18 MΩ) was used to prepare all aqueous solutions. Besides, all chemicals were analytical grade and obtained from commercial suppliers and used without further purification.

2. Electrochemical performance characterizations

The crystal structure of samples was determined by X-ray diffraction (XRD, D8 Advance X-ray diffractometer) operated at 40 kV and 40 mA with a Cu Kα radiation (λ=1.5405 Å) in the 2θ ranging from 5° to 70° with a step size of 0.02°.

The morphology and structure of the samples were performed by a scanning electron microscopy (SEM) at an accelerating voltage of 10 kV. The system is equipped with an EDX detector (129 eV, 60 mm, Octane Silicon Drift Detector, EDAX, AMTEK Inc. USA).

The concentration of the leached Au^{3+} in solution was quantified by an inductively coupled plasma mass spectrometry instrument.

3. Electrochemical nitrate reduction reaction (NO_3RR) measurements

The electrochemical measurements were performed on an electrochemical workstation (Biological VSP-300) with 0.1 M HNO_3 as an electrolyte. Electrochemical analysis was carried out in a H-shape three-electrode quartz cell, among which the Au electrode, a titanium MMO anode mesh (1mm thick x 25mm x 25mm), and saturated calomel electrode (SCE) were employed as the working electrode, counter electrode, and reference electrode, respectively. Counter electrode (titanium MMO anode mesh) and working electrode (Au electrode) were placed in a separate cell separated by a Nafion 117 membrane. The length of gold wire was 5 cm. 0,1 M HNO_3 solution (80 mL) was evenly distributed to the cathode and anode compartment. All the potentials are expressed in reversible hydrogen electrode (RHE) scale using

$$E\ (vs.\ RHE) = E\ (vs.\ SCE) + 0.241 + 0.059 \times pH.$$

The potentiostatic tests were carried out in 0.1 M HNO_3 as the electrolyte at different given potentials for 1 h with a stirring rate of 500 rpm. Linear sweep voltammetry (LSV) experiments were carried out on an electrochemical workstation (Biological VSP-300). The cathodic polarization curves were obtained using the linear sweep voltammetry technique with a scan rate of 0.5 mV s^{-1} in 0.1 M HNO_3 aqueous solution.

For the study of the influence of pH, a solution containing different concentration of H_2SO_4 and 0.1 M KNO_3 was used at an applied potential of −0.7V vs RHE.

4. Hydroxylamine (NH_2OH) and ammonia (NH_3) detection by using ion chromatography

Primary NH_2OH and NH_3 detections and quantifications were carried out by using ion chromatography (Eco IC from Metrohm). NH_2OH calibration curve was made by diluting $NH_2OH{\cdot}HCl$ solution into six different concentrations of NH_2OH (0.1 ppm, 0.2ppm, 0.5ppm, 1ppm, 2ppm and 5ppm). The fitting curve ($A = 0.075C - 3.885 \times 10^{-4}$, $R^2 = 0.99994$) was found to be in linear coherence with the concentration of NH_2OH. Then NH_2OH concentration was quantified by NH_2OH calibration curve.

NH_3 calibration curve was made by diluting 1000 ppm ammonia standard solution into six different concentrations of NH_3 (0.2ppm, 0,5ppm, 1ppm, 2ppm 5ppm and 10ppm). The fitting curve ($A = 0.229C - 2.702 \times 10^{-4}$, $R^2 = 0.99999$) was found to be in linear coherence with the concentration of NH_3. NH_3 concentration was quantified by NH_3 calibration curve.

For nitrate electroreduction, the yield and Faradaic efficiency were calculated by the following equations:

NH_2OH yield rate calculation：

$$Yield_{NH2OH} = (c_{NH2OH} \times V) / (M_{NH2OH} \times t \times S)$$

Calculation of Faradic efficiency (FE) towards NH_2OH

$$Faradaic\ efficiency = (6F \times c_{NH2OH} \times V) / (M_{NH2OH} \times Q)$$

NH_3 yield rate calculation:

$$Yield_{NH3} = (c_{NH3} \times V) / (M_{NH3} \times t \times S)$$

Calculation of Faradic efficiency (FE) towards NH_3

$$\text{Faradaic efficiency} = (8F \times c_{NH3} \times V) / (M_{NH3} \times Q)$$

where c_{NH2OH} and c_{NH3} are the mass concentration of NH_2OH and NH_3 respectively, V is the volume of electrolyte in the cathode compartment, M_{NH2OH} and M_{NH3} are the molar mass of NH_2OH and NH_3 respectively, t is the electrolysis time, S is the geometric area of working electrode, F is the Faradaic constant, Q is the total charge passing the electrode.

5. Ammonia (NH_3) detection by using the indophenol blue method

The concentration of produced NH_3 in the electrolyte was spectrophotometrically determined by the indophenol blue method. In detail, 2 mL of 1 M NaOH solution containing salicylic acid (5 wt.%) and sodium citrate (5 wt.%) was added in 2 mL diluted electrolyte. Subsequently, 1 mL of NaClO solution (0.05 M) and 0.2 mL of sodium nitroferricyanide solution (1 wt.%) were added to the above solution. Absorbance measurements were performed from 500 nm to 800 nm. The concentration-absorbance (at 655 nm) curve was calibrated using standard NH_4^+ solutions with a series of concentrations. The fitting curve ($A = 0.1482C + 0.0306$, $R^2 = 0.9952$) showed a good linear relationship between absorbance value and NH_3 concentration.

6. Hydrogen (H_2) detection by using gas chromatography

Calibration curves for H_2 were established, which were then used to determine the production rates and FE of H_2 in NO_3RR. Various volumes of H_2 were injected directly in the GC (Shimadzu 2014 GC, molecular sieve 5A column, TCD detector) to generate the H_2 calibration curve. The fitting curve ($A = 214829V + 2406$, $R^2 = 0.9984$) demonstrated a strong linear relationship between the peak area and H_2 volume. The electrocatalytic reactions were conducted at -0.7 V vs. RHE in 0.1 M HNO_3 for 1 h, and 1mL of reactive gas was sampled from the reactor with a syringe for analysis using a gas chromatograph.

The yield and Faradaic efficiency of H_2 were calculated by the following equations:

H_2 yield rate calculation：

$$\text{Yield}_{H2} = V_{H2} / (V_m \times t \times S)$$

Calculation of Faradic efficiency (FE) towards H_2:

Faradaic efficiency = n Z F / I t

where V_{H2} is the H_2 volume, V_m is the molar volume of gas, n is the number of moles of H_2 evolution, Z is the needed electrons to produce one H_2 molecule, t is the electrolysis time, S is the geometric area of working electrode, F is the Faradaic constant, t is the time, I is the defined current density.

7. Control experiments

A solution of 250 ppm NH_2OH was prepared in 100 mL of 0.1 M HNO_3. Afterward, 5 mM KNO_2 was added to the solution every 30 minutes. Samples were collected every 10 minutes for subsequent ion chromatography analysis.

8. Calculation methods

The density function theory (DFT) calculations were performed on Vienna *Ab initio* Simulation Package (VASP) code[1, 2]. The interaction of core and electrons was treated by projector augmented wave (PAW) pseudopotential[3, 4] with a cut-off energy of 500 eV. The exchange-correlation function was described by the generalized-gradient approximation-Perdew-Burke-Ernzerhof (GGA-PBE)[5]. The DFT-D3 (BJ) method was used to consider the vdW-dispersion energy-correction[6]. Convergence in geometry optimization was reached when the force on each atom fell below 0.02 eV $Å^{-1}$. The Au with exposed (111) facet was modeled as electrocatalyst surfaces to simulate NO_3^- reduction reaction. A vacuum layer of 18 Å was introduced to eliminate the interaction between two adjacent slabs. The Brillouin zone sampling was performed using Gamma-centered Monkhorst-Pack (MP) grids[7], and the k-point was set as $3\times3\times1$ for all the DFT calculations. The data processing was assisted by VASPKIT[8], QVASP[9] and VESTA[10] software. The Gibbs free energy difference (ΔG) between initial and final states was denoted as:

$\Delta G = \Delta E + \Delta ZPE - T\Delta S$

where E, ZPE, T and S represent the energy from DFT calculation, zero-point energy, temperature (298.15 K) and entropy, respectively[11, 12].

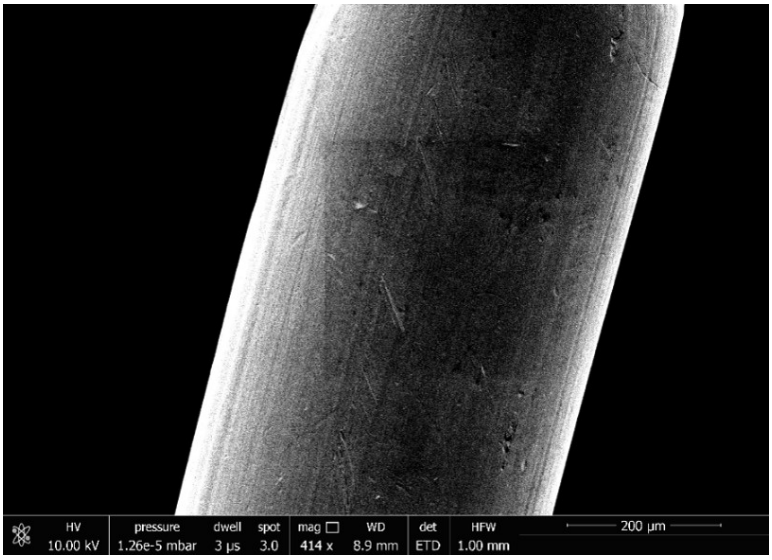

Fig. S1. SEM image of Au wire.

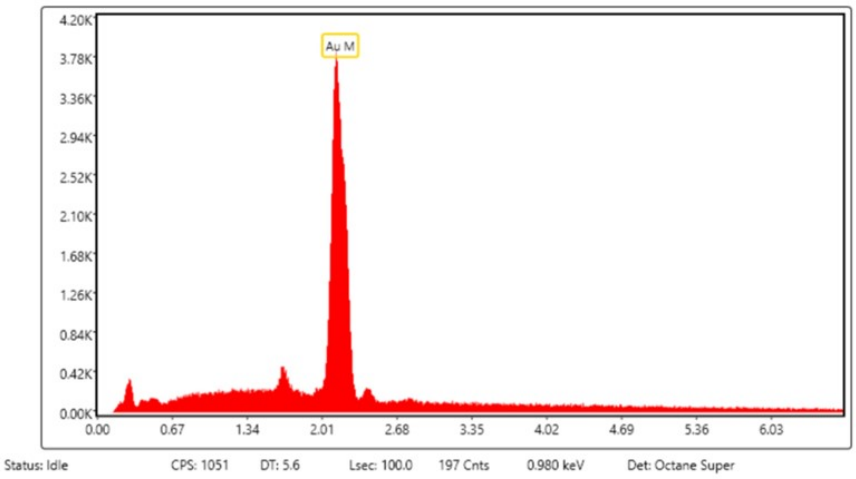

Fig. S2. EDX of Au wire.

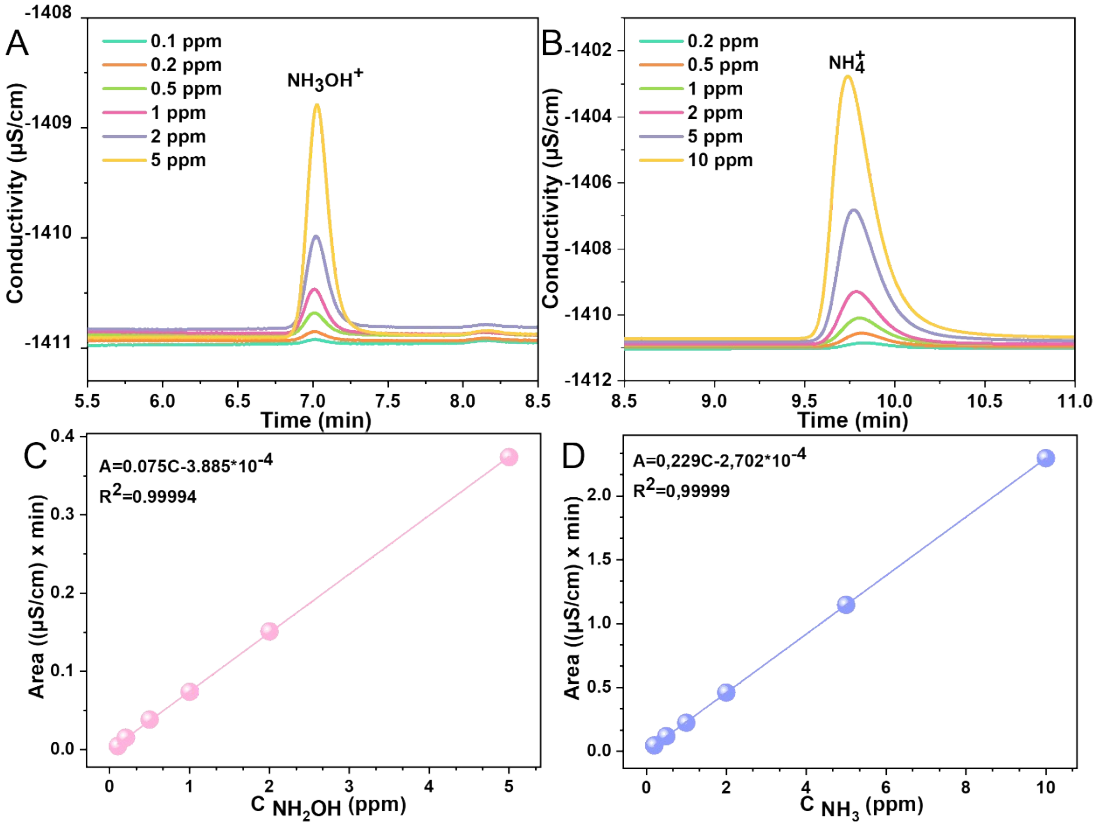

Fig. S3. Ion chromatographic anaylsis of NH_3OH^+ (A) and NH_4^+ (B) at different NH_2OH and NH_3 concentration; the corresponding NH_2OH (C) and NH_3 (D) calibration curves.

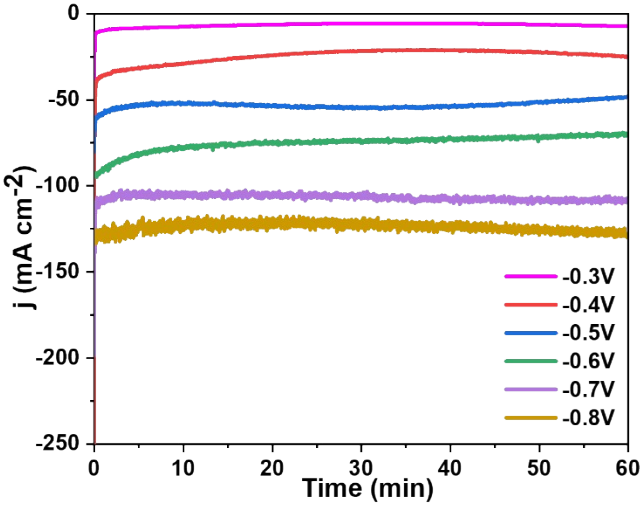

Fig. S4. Chronoamperometry curves of Au wire in 0.1 M HNO_3 at applied potentials for 1 hour.

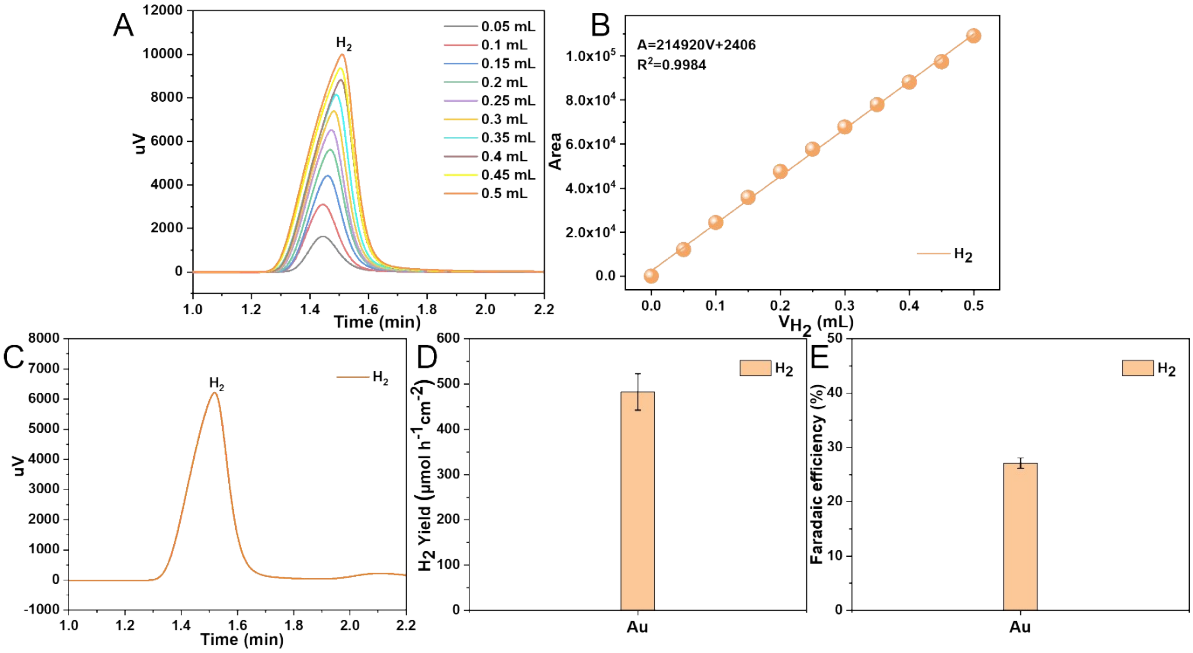

Fig. S5. (A) GC data for generating the calibration curve generated by injecting different H_2 volume; (B) the corresponding H_2 calibration curve; (C) GC curves, (D) H_2 yield and (E) H_2 Faradaic efficiency of Au electrode at an applied potential of -0.7 V vs. RHE in 0.1 M HNO_3 for a period of 1 hour.

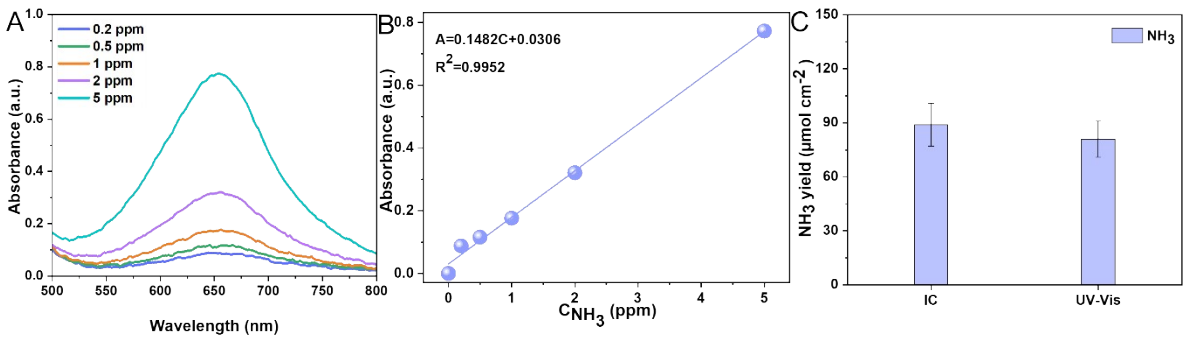

Fig. S6. (A) UV–Vis absorption curves of indophenol assays with ammonia; (B) the corresponding ammonia concentration-absorbance calibration curve; (C) the NH_3 yield rate of Au electrode at -0.7 V vs. RHE quantified by IC and UV–Vis methods for comparative analysis.

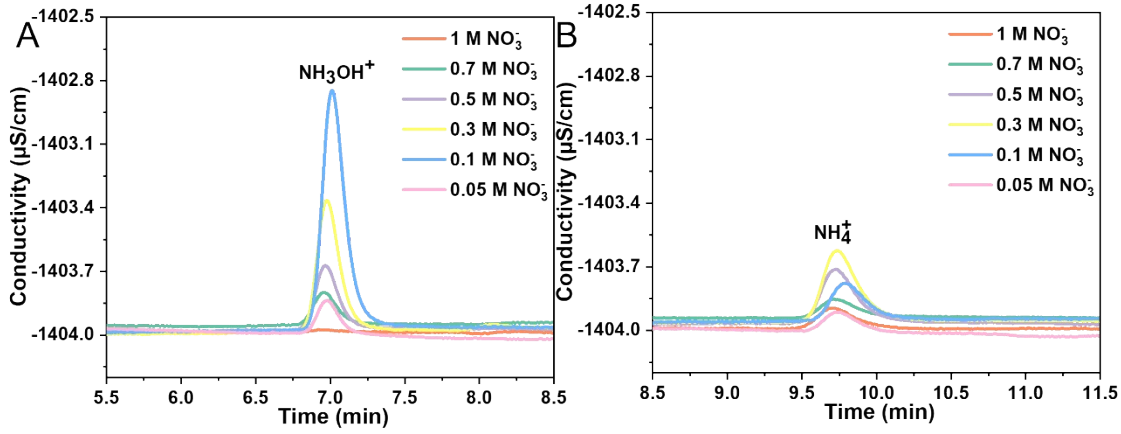

Fig. S7. Ion chromatographic anaylsis of NH_3OH^+ (A) and NH_4^+ (B) at different nitrate concentrations at pH 1; performance assessed at an applied potential of -0.7 V vs. RHE over a 1-hour reaction time.

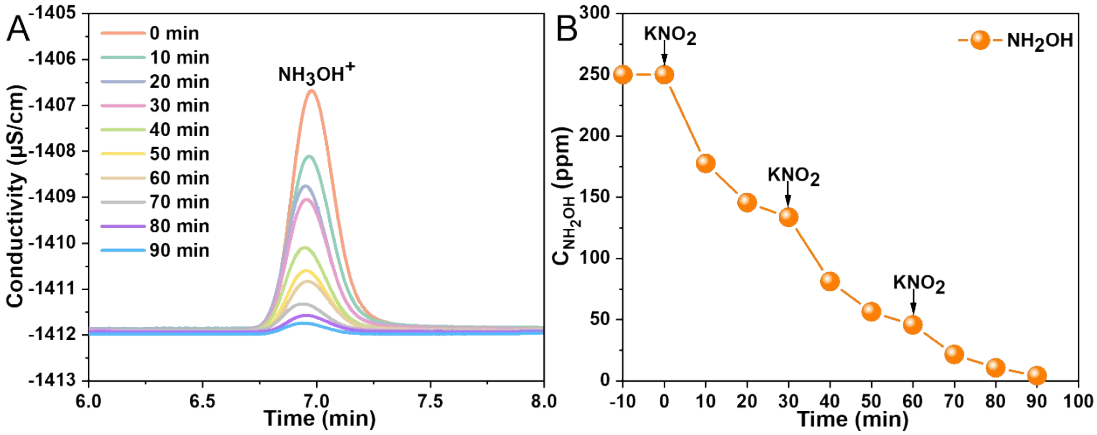

Fig. S8. (A) Ion chromatographic anaylsis of a 0.1 M HNO_3 solutions containing 250 ppm NH_2OH at different time after the addition of KNO_2; (B) NH_2OH concentration over time in 0.1 M HNO_3 solutions after adding KNO_2.

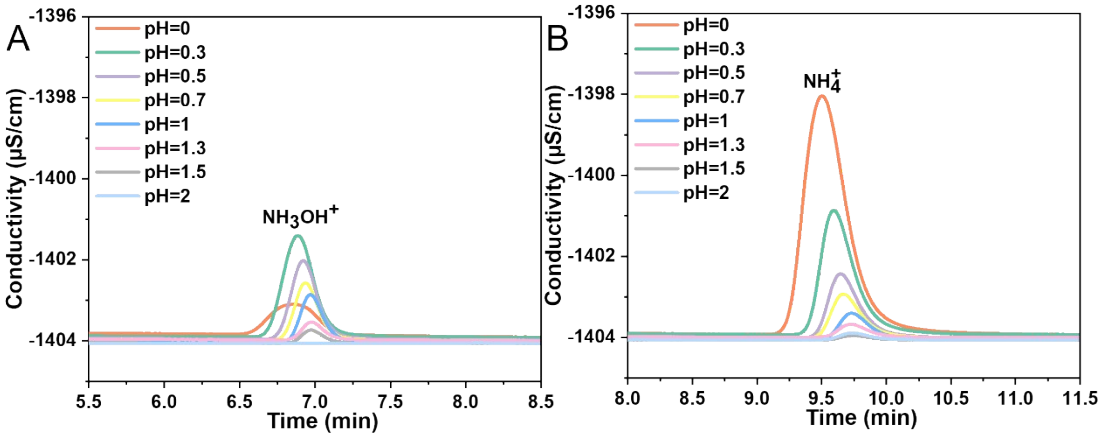

Fig. S9. Ion chromatographic anaylsis of NH_3OH^+ (A) and NH_4^+ (B) across various pH levels, assessed in a solution of 0.1 M KNO_3 with H_2SO_4 adjusting the pH, at an applied potential of -0.7 V vs. RHE for a period of 1 hour.

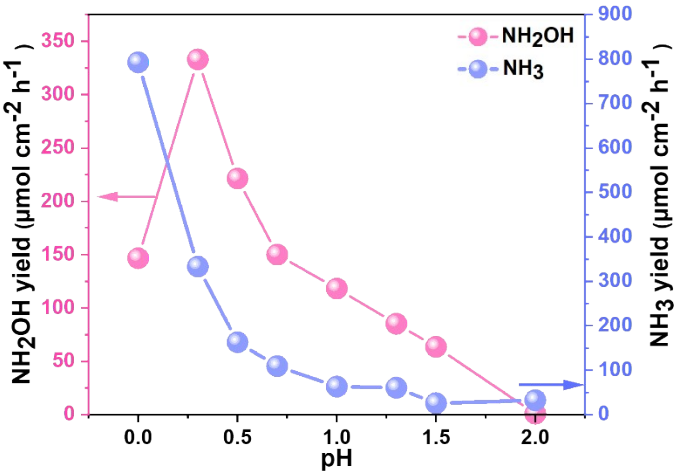

Fig. S10. Yield rates of NH_2OH and NH_3 across various pH levels, assessed in a solution of 0.1 M KNO_3 with H_2SO_4 adjusting the pH, at an applied potential of -0.7 V vs RHE for a period of 1 hour.

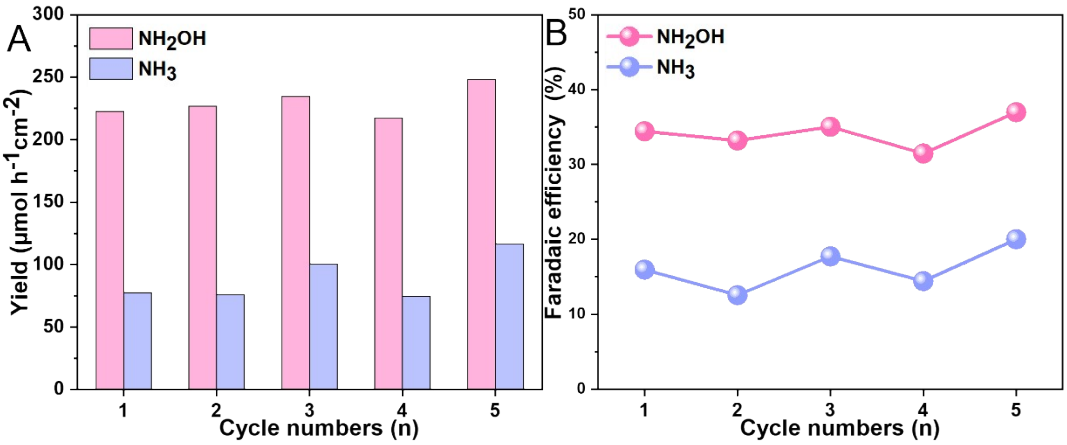

Fig. S11. Stability test results for the Au electrode. NH_2OH and NH_3 yield rate (A) and Faradaic efficiency (B) of Au electrode at -0.7 V vs. RHE in 0.1 M HNO_3 in different cycles.

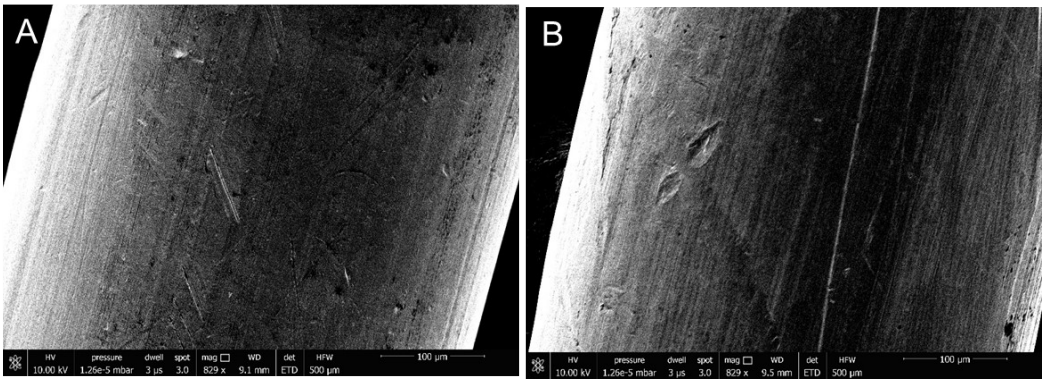

Fig. S12. SEM images of Au wire before (A) and after (B) test.

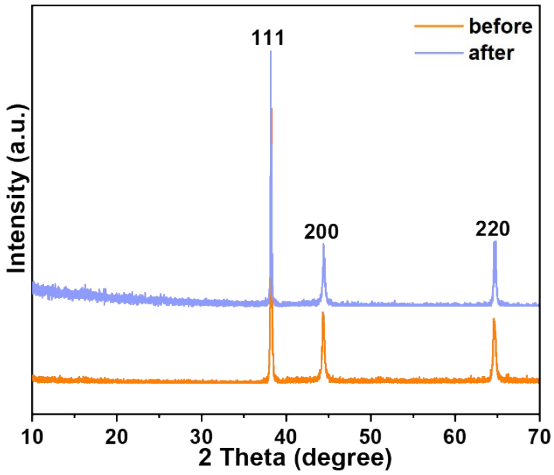

Fig. S13. XRD pattern of Au wire before and after test.

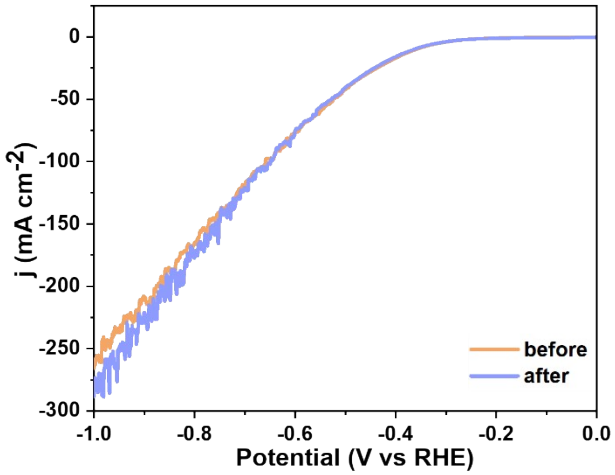

Fig. S14. LSV curves of Au wire before and after test.

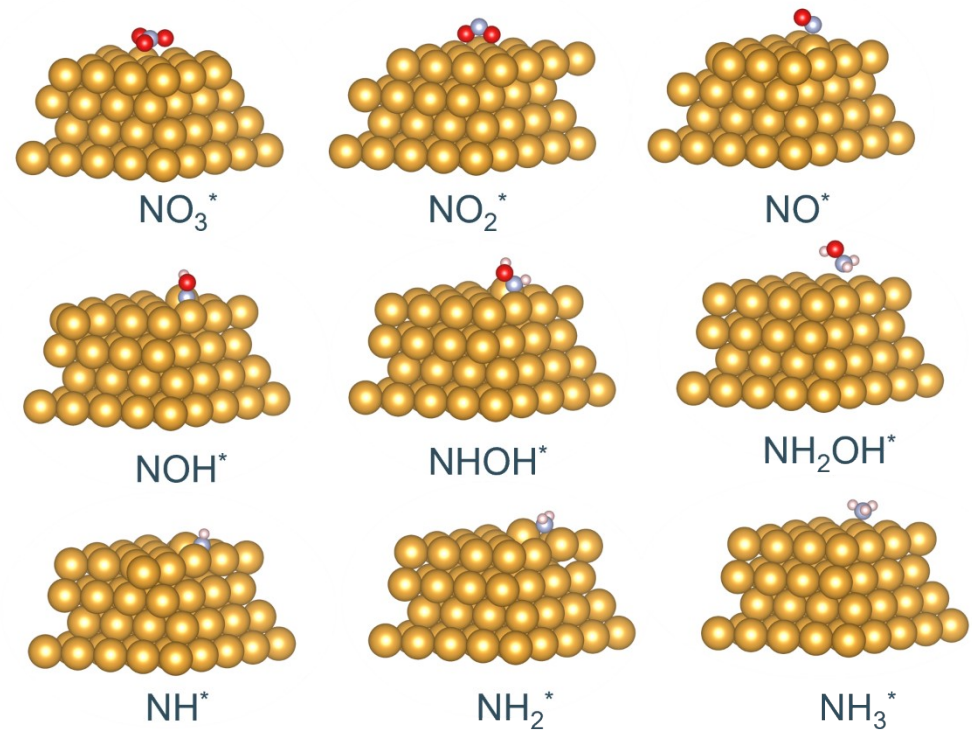

Fig. S15. The reaction intermediate adsorption configurations of NO_3RR to NH_2OH and NH_3 on the Au surface. The red, pink, gray and yellow balls represent oxygen, hydrogen, nitrogen and gold atoms, respectively.

Table S1. The measured pH of electrolytes before and after reaction under different nitrate concentration in 0.1 M HNO_3 at -0.7 V vs. RHE for 2 hour

Concentration of Nitrate	pH		
	before	After	Changed
0.1 M	1.19	1.30	0.11
0.3 M	1.28	1.73	0.45
0.5 M	1.28	1.96	0.68
0.7 M	1.27	2.20	0.93
1 M	1.25	2.74	1.49

Table S2. The ICP analysis of leakage Au^{3+} before and after test

Samples	Leakage	
	Condition	Au^{3+} (mg/L)
Electrolyte	before	N.D.
Au wire	after	N.D.

Note: N.D. = Not Detected.

Table S3. Free energy of various intermediates on Au, setting the first adsorbed state as the reference level.

Reactant/Intermediates	Energy (eV)
NO_3^-	0.00
NO_3*	-0.75
NO_2*	-2.91
NO*	-3.50
NOH*	-3.15
NHOH*	-3.97
NH_2OH*	-4.90
NH_2OH	-6.60
NH*	-4.46
NH_2*	-6,23
NH_3*	-7.34
NH_3	-7.98

Table S4. Comparison of the rate-determining step (RDS) of Au wire with other reported electrocatalysts for NO_3RR.

Catalysts	RDS	Energy	Reference
Au	NO*→ NOH*	0.35 eV	This work
Cu/Cu_2O	NO*→ NOH*	0.84 eV	[13]
PdCu	NO*→ NOH*	0.53 eV	[14]
PdCo		0.64 eV	
PdFe		0.75 eV	
PdNi		0.89 eV	
Pd		0.92 eV	
FePc	NO*→ NOH*	0.85 eV	[15]
$FePc/TiO_2$		0.74 eV	
Ni	NO*→ NOH*	0.37 eV	[16]
Rh		0.39 eV	
Pd		0.72 eV	
Fcc Pd (100)	NO*→ NOH*	0.45 eV	[17]
Fe_3C	NO*→ NOH*	1.74 eV	[18]
Fe_3C-Cu_3		1.28 eV	

References

1. G. Kresse and J. Furthmüller, *Comput. Phys. Commun.*, 1996, **6**, 15-50.
2. G. Kresse and J. Furthmüller, *Phys. Rev. B*, 1996, **54**, 11169-11186.
3. G. Kresse and D. Joubert, *Phys. Rev. B*, 1999, **59**, 1758-1775.
4. P. E. Blöchl, *Phys. Rev. B*, 1994, **50**, 17953-17979.
5. J. P. Perdew, K. Burke and M. Ernzerhof, *Phys. Rev. Lett.*, 1996, **77**, 3865-3868.
6. S. Grimme, S. Ehrlich and L. Goerigk, *J. Comput. Chem.*, 2011, **32**, 1456-1465.
7. D. J. Chadi and M. L. Cohen, *Phys. Rev. B*, 1973, **8**, 5747-5753.
8. V. Wang, N. Xu, J.-C. Liu, G. Tang and W.-T. Geng, *Comput. Phys. Commun.*, 2021, **267**, 108033.
9. W. Yi, G. Tang, X. Chen, B. Yang and X. Liu, *Comput. Phys. Commun.*, 2020, **257**, 107535.
10. K. Momma and F. Izumi, *J. Appl. Crystallogr.*, 2011, **44**, 1272-1276.
11. J. K. Nørskov, J. Rossmeisl, A. Logadottir, L. Lindqvist, J. R. Kitchin, T. Bligaard and H. Jónsson, *J. Phys. Chem. B*, 2004, **108**, 17886-17892.
12. J. Zhang, J. Ma, T. S. Choksi, D. Zhou, S. Han, Y.-F. Liao, H. B. Yang, D. Liu, Z. Zeng, W. Liu, X. Sun, T. Zhang and B. Liu, *J. Am. Chem. Soc.*, 2022, **144**, 2255-2263.
13. N. Zhou, Z. Wang, N. Zhang, D. Bao, H. Zhong and X. Zhang, *ACS Catal.*, 2023, **13**, 7529-7537.
14. Y. Zhou, L. Zhang, Z. Zhu, M. Wang, N. Li, T. Qian, C. Yan and J. Lu, *Angew. Chem. Int. Ed. Engl.*, 2024, **63**, e202319029.
15. R. Zhang, C. Li, H. Cui, Y. Wang, S. Zhang, P. Li, Y. Hou, Y. Guo, G. Liang, Z. Huang, C. Peng and C. Zhi, *Nat Commun*, 2023, **14**, 8036.
16. M. Karamad, T. J. Goncalves, S. Jimenez-Villegas, I. D. Gates and S. Siahrostami, *Faraday Discuss.*, 2023, **243**, 502-519.
17. M. Xie, S. Tang, Z. Li, M. Wang, Z. Jin, P. Li, X. Zhan, H. Zhou and G. Yu, *J. Am. Chem. Soc.*, 2023, **145**, 13957-13967.
18. Y. Hua, N. Song, Z. Wu, Y. Lan, H. Luo, Q. Song and J. Yang, *Adv. Funct. Mater.*, 2024, **34**.